

Dalton Transactions

Accepted Manuscript



This is an *Accepted Manuscript*, which has been through the Royal Society of Chemistry peer review process and has been accepted for publication.

Accepted Manuscripts are published online shortly after acceptance, before technical editing, formatting and proof reading. Using this free service, authors can make their results available to the community, in citable form, before we publish the edited article. We will replace this *Accepted Manuscript* with the edited and formatted *Advance Article* as soon as it is available.

You can find more information about *Accepted Manuscripts* in the [Information for Authors](#).

Please note that technical editing may introduce minor changes to the text and/or graphics, which may alter content. The journal's standard [Terms & Conditions](#) and the [Ethical guidelines](#) still apply. In no event shall the Royal Society of Chemistry be held responsible for any errors or omissions in this *Accepted Manuscript* or any consequences arising from the use of any information it contains.

Heteroleptic Platinum(II) Isocyanide Complexes: Convenient Synthetic Access, Polymorphs, and Vapoluminescence

Cite this: DOI: 10.1039/x0xx00000x

Daron E. Janzen,^{*a} and Kent R. Mann^bReceived 00th January 2012,
Accepted 00th January 2012

DOI: 10.1039/x0xx00000x

www.rsc.org/

A convenient synthetic scheme was developed to access a series of square-planar Pt(II) complexes of the form (TBA)[Pt(CN)₃(CNR)] (TBA= tetra-*n*-butyl ammonium cation, R = CH₃, *c*-C₆H₁₁, *p*-C₆H₄-C₂H₅). These heteroleptic complexes were characterized by combustion analyses, single-crystal X-ray structure determinations, HRFAB-MS, ¹H NMR, ATR-IR, solution UV-Vis, and solid-state emission spectroscopies. Surprisingly, each of these complexes exhibit low energy room temperature solid-state luminescence in the absence of intermolecular Pt-Pt interactions. Additionally, the polymorphic behavior of (TBA)[Pt(CN)₃(CN-*c*-C₆H₁₁)] was elucidated through a combination of single-crystal X-ray structure determinations, X-ray powder diffraction, and mass uptake experiments. Vapoluminescence and polymorphic transformations of (TBA)[Pt(CN)₃(CN-*c*-C₆H₁₁)] were concomitant with water vapor absorption. A new double-salt complex [Pt(terpy)Cl][Pt(CN)₃(CNCH₃)] (terpy = 2,2'-5',2''-terpyridine) was also synthesized and characterized by combustion analysis, ATR-IR, HRFAB-MS, and solid-state UV-Vis and emission spectroscopies. The vapoluminescent properties of this salt in response to water were examined by mass uptake experiments, ATR-IR, and solid-state emission spectroscopy. A principal component analysis (PCA) of the solid-state emission changes induced by water vapor confirmed the presence of an intermediate emissive species.

Introduction

Vapochromism and vapoluminescence are properties of solid-state materials that involve changes in the electronic spectra or luminescence spectra upon exposure to vapors of volatile organic compounds (VOCs) or water. Potential applications of vapochromic materials include sensor devices for detection of VOCs and water in the lab or natural environment, process control uses such as pharmaceutical or food manufacturing, and remote monitoring in hazardous locations.

^aDepartment of Chemistry and Biochemistry, St. Catherine University, 2004 Randolph Avenue, St. Paul, MN, USA. E-mail: dejanzen@stkate.edu; Fax: +1651-690-8657; Tel.: +1651-690-6047

^bDepartment of Chemistry, University of Minnesota, 207 Pleasant St. SE, Minneapolis, MN, USA.

†Electronic supplementary information (ESI) available: Crystallographic and spectroscopic data. CCDC Data for the X-ray crystal structures 1035788-1035791. For ESI and crystallographic data in CIF or other electronic format see DOI:XXXXXXXXXX

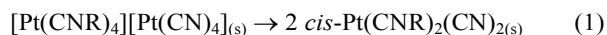
Interest in vapochromic and vapoluminescent complexes has grown tremendously in recent years,¹ with numerous types of coordination compounds and organometallic complexes reported with these properties, most of these involving either d⁸ Pt(II) or d¹⁰ Au(I) systems. Though much of our early work focused on mechanistic aspects of the vapochromic response,^{2,3,4,5} we have also developed practical vapochromic sensor devices including an “electronic nose” to discriminate between different VOCs,⁶ a dual quartz crystal microbalance (QCM) and optical reflectance sensor,⁷ and have shown a proof of concept material capable of chiral analyte discrimination.⁸

Unlike many other types of vapochromic and vapoluminescent complexes, the double-salt ([Pt(CNR)₄][Pt(CN)₄]) and neutral compounds (*cis*-Pt(CNR)₂(CN)₂) (where R = alkyl, aryl) we have studied undergo large reversible spectroscopic changes. In these vapochromic materials, alterations in intermolecular Pt-Pt interactions accompany crystalline phase changes caused by the sorption of guest molecules, giving rise to the observed spectroscopic changes.^{5,9,10} The insolubility of the dication/dianion vapochromic double-salt materials is favorable

for sensing of a wide variety of volatiles, but also limits purification strategies and single crystal X-ray structural characterization possibilities. Poor solubility also leads to difficulties involving materials processing that would be desirable for sensing devices, such as casting thin homogeneous films. The higher solubility of the neutral vapochromic complexes mitigates these problems associated with the double-salt complexes, but also limits the exposure of these complexes to exclude certain guest molecules that may dissolve or recast an optical film of the material.

Square-planar complexes of the same type (mixed cyanide/isocyanide complexes of Pt(II)) with intermediate electrostatic interactions might result in the combination of the best properties of both neutral and double-salt vapochromic materials. One strategy is to employ combinations of monocations and monoanions to form double salt complexes with reduced electrostatic interactions relative to the dication/dianion salts. Monocations and monoanions of the forms $[\text{Pt}(\text{CNR})_3(\text{CN})]^+$ and $[\text{Pt}(\text{CN})_3(\text{CNR})]^-$ are largely unknown and obvious generic synthetic routes are unclear.¹¹

Neutral complexes of the form *cis*-Pt(CNR)₂(CN)₂ (where R = alkyl, aryl) are readily prepared by heating the related solid double salt complex $[\text{Pt}(\text{CNR})_4][\text{Pt}(\text{CN})_4]$ to its melting temperature in the absence of solvent as is shown in Reaction 1.⁹



When purifying the crude product of this melt reaction with R=CN-*p*-(C₂H₅)C₆H₄ using chromatography, a small quantity of a previously unidentified compound was separated from the desired neutral species. Subsequent growth of crystals and a single crystal X-ray structure revealed this minor product was the TBA⁺ (TBA = tetra-*n*-butyl ammonium cation) salt of a monoanionic complex $[\text{Pt}(\text{CN})_3(\text{CN-}i>p\text{-}(\text{C}_2\text{H}_5)\text{C}_6\text{H}_4)]^-$. Presumably, the TBA⁺ was carried over as an impurity in the synthesis of the double-salt. This led us to develop a rational synthesis of other monoanions with three cyanide ligands and one isocyanide ligand, for use in preparing monoanion/monocation double salt complexes.

Reported here are a series of Pt(II) monoanionic complexes of the form (TBA)[Pt(CN)₃(CNR)] (where R = CH₃, *c*-C₆H₁₁, *p*-(C₂H₅)-C₆H₄). Interesting room temperature solid-state emission properties of these monoanions and the relation to their X-ray crystal structures is discussed. X-ray powder diffraction studies of two different polymorphs of a particular anion $[\text{Pt}(\text{CN})_3(\text{CN-}i>c\text{-}(\text{C}_6\text{H}_{11}))]^-$ have also been carried out. A new type of monocation/moanion double-salt complex $[\text{Pt}(\text{terpy})\text{Cl}][\text{Pt}(\text{CN})_3(\text{CNCH}_3)]$ (terpy = 2,2':6',2''-terpyridine) has been synthesized and its potential as a water sensor has been explored. Principal component analysis (PCA) of the emission behavior of this complex reveals the presence of an intermediate hydrated species that gravimetric experiments could not detect.

Experimental

General Considerations

K₂[PtCl₄] was purchased from Colonial Metals. (TBA)₂[Pt(CN)₄] was prepared from (TBA)Br (Aldrich) and K₂[Pt(CN)₄] (Colonial Metals) as previously reported.¹² The complexes $[\text{Pt}(\text{CNCH}_3)_4][\text{Pt}(\text{CN})_4]$,¹³ *cis*-Pt(CN-*p*-(C₂H₅)C₆H₄)₂(CN)₂,⁹ $[\text{Pt}(\text{CN-}i>c\text{-}(\text{C}_6\text{H}_{11}))][\text{Pt}(\text{CN})_4]$,¹⁴ and $[\text{Pt}(\text{terpy})\text{Cl}]\text{Cl}$ ¹⁵ were prepared as previously reported. All solvents used were of ACS reagent grade and used as received. The chloroform and 1,2-dichloroethane solvents used were stabilized with amlenes. Combustion analyses were performed by QTI Analytical Laboratories. High resolution FAB mass spectral measurements of the metal complexes in a *m*-nitrobenzyl alcohol matrix were obtained with a VG Analytical 7070E-HF instrument. Infrared absorption spectra were obtained using the attenuated total reflectance (ATR) method on a Nicolet Magna-IR System 550 spectrometer equipped with a ZnSe trough HATR cell from PIKE Technologies. Data were processed with OMNIC ESP v.4.1 software. ¹H NMR spectra were recorded on a Varian VXR-300 or VI-300 MHz instrument. Chemical shifts are reported in parts per million (ppm) and referenced to the residual dichloromethane solvent peak (5.32 ppm). Solution UV-Vis absorption spectra were acquired using a computer controlled Cary 17 in dichloromethane. Solid UV-Vis absorption spectra were acquired as films cast from a diethyl ether suspension of the solid sample (**4**) on a custom built zirconium oxide attenuated total reflectance (ATR) crystal. A correction was applied to all solid UV-Vis spectra to account for the effect of penetration depth on wavelength. Emission spectra were acquired at room temperature using either an Ocean Optics CCD array spectrometer or a Princeton Instruments ST138 UV-Vis/NIR sensitive liquid nitrogen cooled/CCD spectrometer. Solid emission spectra collected on the Princeton Instruments spectrometer (front-face detection) were collected from samples irradiated at 477 nm with an LED using the Winspec v1.6.1.3 software package. Solid emission spectra collected on the Ocean Optics spectrometer (front-face detection) were collected from samples irradiated at 405 nm (**1,2,3**) or 477 nm (**4**) with an LED using the OOIBase32 program. The emission spectra taken using the Princeton Instruments CCD were corrected for grating efficiency and detector response. Emission spectra acquired using the Ocean Optics CCD were not corrected. Relative humidities are reported in percent relative humidity and were measured using a Decagon CX-2 humidity measurement apparatus.

Synthesis

(TBA)[Pt(CN)₃(CNCH₃)] (**1**)

To a solution of (TBA)₂[Pt(CN)₄] (0.717 g, 0.914 mmol) in CHCl₃ was added $[\text{Pt}(\text{CNCH}_3)_4][\text{Pt}(\text{CN})_4]$ (0.301 g, 0.457 mmol). The resulting suspension was heated at reflux for 4d, at which time all solids were dissolved. The solvent was removed in vacuo, and the crude reaction mixture was purified by silica gel chromatography (5% MeOH in CH₂Cl₂). The first fraction was collected, the solvent was removed in vacuo, and then

redissolved in CH_2Cl_2 (10 mL). Addition of diethyl ether (300 mL) provided a pale yellow precipitate which was collected, rinsed with diethyl ether, and dried. Yield: 0.683 g, 1.23 mmol, 69%. Anal. Calcd. for $\text{C}_{21}\text{H}_{39}\text{N}_5\text{Pt}\cdot\text{H}_2\text{O}$: C, 43.89; H, 7.19; N, 12.19. Found: C, 44.21; H, 6.95; N, 12.15. IR (ATR, cm^{-1}): $\nu(\text{CNR}) = 2257$, $\nu(\text{CN}) = 2158, 2147, 2137$. UV-Vis (CH_2Cl_2 solution, nm ($\epsilon / (\text{M}^{-1}\text{cm}^{-1})$)): 260 (11200), 284 (2000). HRFABMS Calcd. for $\text{C}_5\text{H}_3\text{N}_4^{194}\text{Pt} [\text{M} - \text{TBA}]^-$ 312.9985; found, 312.9956. ^1H NMR (300 MHz, CD_2Cl_2) δ 3.45 (t, 3H, $^3J_{\text{Pt-H}} = 6.9$ Hz), 3.19 (m, 8H), 1.66 (m, 8H), 1.44 (m, 8H), 1.02 (t, 12H, $J = 7.5$ Hz).

(TBA)[Pt(CN)₃(CN-*c*-C₆H₁₁)] (2)

Solid $[\text{Pt}(\text{CN}-\text{c}-\text{C}_6\text{H}_{11})_4][\text{Pt}(\text{CN})_4]$ (0.5 g, 0.537 mmol) was heated under nitrogen to the melting point (180°C) and then cooled to rt. A solution of $(\text{TBA})_2[\text{Pt}(\text{CN})_4]$ (0.842 g, 1.07 mmol) in 1,2-dichloroethane was added to the residue from the melt reaction and the mixture was heated at reflux for 3 d. The solvent was removed in vacuo, and the crude reaction mixture was purified by silica gel chromatography using 100% CH_2Cl_2 followed by a gradient of up to 20% CH_3CN in CH_2Cl_2 . The first fraction was collected and the solvent was removed in vacuo giving an oil. The oil was redissolved in $\text{CH}_2\text{Cl}_2/\text{CH}_3\text{CN}$ (1:1, 10 mL), diethyl ether (300 mL) was added, and a oily solution formed. A part of the cloudy solution above the oil (200 mL) was decanted and cooled at 0°C overnight. A seed crystal was harvested from the cold decanted solution and mixed into the oil, causing crystallization. A yellow solid was recovered, rinsed with diethyl ether (50 mL) and dried. Yield: 0.621 g, 0.994 mmol, 46%. Anal. Calcd. for $\text{C}_{26}\text{H}_{47}\text{N}_5\text{Pt}\cdot\text{H}_2\text{O}$: C, 48.58; H, 7.68; N, 10.90. Found: C, 48.59; H, 7.47; N, 10.68. IR (ATR, cm^{-1}): $\nu(\text{CNR}) = 2231$, $\nu(\text{CN}) = 2155, 2145, 2135$. UV-Vis (CH_2Cl_2 solution, nm ($\epsilon / (\text{M}^{-1}\text{cm}^{-1})$)): 261 (13900), 283 (2000). HRFABMS Calcd. for $\text{C}_{10}\text{H}_{11}\text{N}_4^{194}\text{Pt} [\text{M} - \text{TBA}]^-$, 381.0610; found, 381.0643. ^1H NMR (300 MHz, CD_2Cl_2) δ 3.96 (1H), 3.21 (t, 8H, $J = 8.4$ Hz), 1.93 (2H), 1.77 (4H), 1.66 (m, 8H), 1.49 (m, 12H), 1.02 (t, 12H, $J = 7.2$ Hz).

(TBA)[Pt(CN)₃(CN-*p*-(C₂H₅)C₆H₄)] (3)

To a solution of $(\text{TBA})_2[\text{Pt}(\text{CN})_4]$ (0.769 g, 0.981 mmol) in 1,2-dichloroethane was added *cis*- $\text{Pt}(\text{CN}-\text{p}-(\text{C}_2\text{H}_5)\text{C}_6\text{H}_4)_2(\text{CN})_2$ (0.5 g, 0.981 mmol). The resulting solution was heated at reflux for 5 d. The solvent was removed in vacuo, and the crude reaction mixture was purified by silica gel chromatography using 100% CH_2Cl_2 followed by a gradient up to 40% CH_3CN in CH_2Cl_2 . The second fraction was collected, the solvent was removed in vacuo, and then redissolved in CH_3CN (10 mL). Addition of diethyl ether (300 mL) provided a white precipitate which was collected, rinsed with diethyl ether, and dried. Yield: 0.608 g, 0.940 mmol, 48%. Anal. Calcd. for $\text{C}_{28}\text{H}_{45}\text{N}_5\text{Pt}\cdot\text{H}_2\text{O}$: C, 52.00; H, 7.01; N, 10.83. Found: C, 51.72; H, 6.87; N, 10.68. IR (ATR, cm^{-1}): $\nu(\text{CNR}) = 2213$, $\nu(\text{CN}) = 2157, 2149, 2138$. UV-Vis (CH_2Cl_2 solution, nm ($\epsilon / (\text{M}^{-1}\text{cm}^{-1})$)): 273 (19000), 291 (4600). HRFABMS Calcd. for $\text{C}_{12}\text{H}_9\text{N}_4^{194}\text{Pt} [\text{M} - \text{TBA}]^-$, 403.0454; found, 403.0488. ^1H NMR (300 MHz, CD_2Cl_2) δ 7.43 (d, 2H, $J = 8.4$ Hz), 7.30 (d, 2H, $J = 8.4$ Hz), 3.21 (m, 8H), 2.70 (q, 2H, $J = 7.5$ Hz), 1.46 (m, 8H), 1.23 (t, 3H, $J = 7.5$ Hz), 1.03 (t, 12H, $J = 7.2$ Hz).

[Pt(TERPY)Cl][Pt(CN)₃(CNCH₃)] (4)

A solution of $[\text{Pt}(\text{terpy})\text{Cl}]\text{Cl}$ (0.224 g, 0.450 mmol) in water (25 mL) was added to a solution of $(\text{TBA})[\text{Pt}(\text{CN})_3(\text{CNCH}_3)]$ (0.25 g, 0.450 mmol) in acetone (10 mL). A burgundy precipitate formed immediately and the solution was stirred for 2 h. The solid was collected and rinsed with water, acetone, and diethyl ether. The solid appeared orange after drying in vacuo. Yield: 0.309 g, 0.397 mmol, 89%. Anal. Calcd. for $\text{C}_{20}\text{H}_{14}\text{ClN}_7\text{Pt}_2$: C, 30.88; H, 1.81; N, 12.60. Found: C, 30.78; H, 1.41; N, 12.31. IR (ATR, cm^{-1}): $\nu(\text{CNR}) = 2267$, $\nu(\text{CN}) = 2157, 2148, 2131$. HRFABMS Calcd. for $\text{C}_{15}\text{H}_{11}\text{N}_3^{194}\text{Pt}^{35}\text{Cl} [\text{M}-[\text{Pt}(\text{CN})_3(\text{CNCH}_3)]]^+$, 462.0268; found, 462.0274. HRFABMS Calcd. for $\text{C}_5\text{H}_3\text{N}_4^{194}\text{Pt} [\text{M}-[\text{Pt}(\text{terpy})\text{Cl}]]^-$, 312.9985; found, 313.0000.

X-ray Structure Determinations

Single crystals were attached to glass fibers and mounted on the Siemens SMART¹⁶ system for data collection using graphite-monochromated Mo K α radiation ($\lambda = 0.71073$ Å). The intensity data were corrected for absorption and decay using SADABS¹⁷ or TWINABS.¹⁸ Space groups were determined on the basis of systematic absences and intensity statistics. Direct-methods solutions provided the positions of most non-hydrogen atoms. Several full-matrix least-squares/difference Fourier cycles were performed to locate the remaining non-hydrogen atoms. All calculations were performed using the SHELXTL-V5.0 suite of programs.¹⁹ Crystal and X-ray collection and refinement data for all structures is summarized in Table S1. Figures were prepared using ORTEP-3²⁰ and POV-RAY.²¹

(TBA)[Pt(CN)₃(CNCH₃)] (1)

Suitable colorless X-ray quality single crystals of **1** were grown from an acetonitrile/diethyl ether mixture at -15 °C overnight. A thermal ellipsoid diagram of the anion of **1** is shown in Fig. 1. Compound **1** crystallized in the relatively uncommon polar space group P4₁2₁2. The refined Flack parameter (-0.005(12)) indicated the absolute structure relative to the polar axes was well determined. No solvent molecules were present in the structure. The atoms Pt1, C1, N1, C3, N3 are all on special positions with two-fold site symmetry. An isomorphous structure of **1** has been previously reported¹¹ with data collected at rt.

(TBA)[Pt(CN)₃(CN-*c*-C₆H₁₁)] (2)

Two different polymorphs of **2** were crystallized and examined by single-crystal structure determinations. A colorless polymorph **2-c** and an orange polymorph **2-o** were grown under different conditions. Suitable quality single crystals of **2-c** were grown from an acetonitrile/diethyl ether mixture at room temperature over two months. Single crystals of **2-o** were grown from an acetonitrile/diethyl ether mixture at room temperature which evaporated over two weeks to form viscous colorless islands which slowly transformed into orange crystalline material after an additional one month. Upon mounting a crystal of **2-c** and cooling to -100°C, a destructive phase change occurred within 20 minutes. A new crystal of **2-c** was cooled to -50°C, at which the crystal was stable and the data collection proceeded normally. No decay of the crystal

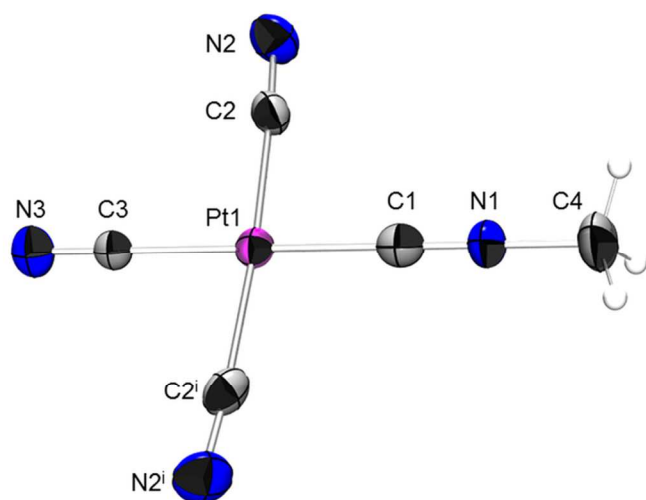


Fig. 1 Thermal ellipsoid diagram of the anion of (TBA)[Pt(CN)₃(CNCH₃)] (**1**) (50% probability ellipsoids, cation omitted for clarity, symmetry code $i=1-y, 1-x, 0.5-z$)

was evident upon comparing redundant data taken early and towards the end of the data collection. Crystals of **2-o** were stable at -100°C and the data collection was performed at -100°C .

A thermal ellipsoid diagram of the anion of **2-c** is shown in Fig. 2. No solvent molecules were found in the structure. A thermal ellipsoid diagram of the anion of **2-o** is shown in Fig. 3. For **2-o**, the refinement stalled at $R_1 = 0.1017$, at which point signs of twinning were noticed. The data were re-integrated²² and the absorption correction was reapplied.¹⁸ The non-merohedral twin law, $[0.95764 \ -0.03321 \ -0.06133 \ / \ 0.00086 \ 0.99556 \ -0.01278 \ / \ 0.13075 \ 0.05759 \ 1.03489]$, a -3.545° rotation about direct lattice axis $[-0.90215, -3, -2.05589]$ and reciprocal lattice axis $[0.92533, -3, -1.71661]$, was determined from program GEMINI.²³ Additional reflection

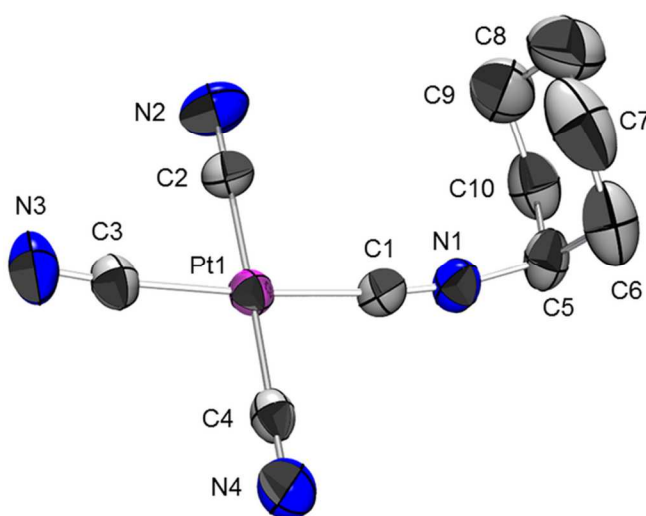


Fig. 2 Thermal ellipsoid diagram of the anion of the colorless polymorph of (TBA)[Pt(CN)₃(CN-*c*-C₆H₁₁)] **2-c** (50% probability ellipsoids, cations and hydrogens omitted for clarity).

manipulation was accomplished using program STRIP-REDUNDANT,²⁴ which removed redundant reflections produced by program TWINABS. In addition, systematic absence violations were removed using program SYSABSFILTER.²⁵ There were 11717 reflections associated solely with the major twin component, 11543 reflections associated solely with the minor twin component, and 1991 overlapping reflections. The final twin component ratio refined to 55:45. Residual electron density peaks varying from 5.86 to 2.36 electrons per \AA^3 are located approximately 1.0 \AA from the Pt atoms, and are likely due to Fourier truncation. Three restraints were employed in the final solution. Atoms C2, C3, C4 were restrained to have the same anisotropic thermal displacement parameters.

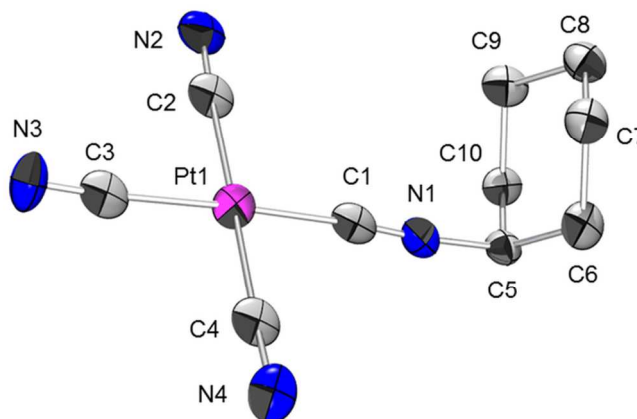


Fig. 3 Thermal ellipsoid diagram of the anion of the orange polymorph of (TBA)[Pt(CN)₃(CN-*c*-C₆H₁₁)] **2-o** (50% probability ellipsoids, cations and hydrogens omitted for clarity).

Atoms C11, C15, C19, C23 were also restrained to have identical thermal parameters. Atoms Pt1, C1, N1 were subjected to a 'rigid bond' restraint. Data collection and refinement parameters for **2-o** and **2-c** are in Table 1.

(TBA)[Pt(CN)₃(CN-*p*-(C₂H₅)C₆H₄)] (**3**)

Suitable yellow X-ray quality single crystals of **3** were grown from an acetonitrile/diethyl ether mixture at -15°C overnight. A thermal ellipsoid diagram of the anion of (TBA)[Pt(CN)₃(CN-*p*-(C₂H₅)C₆H₄)] is shown in Fig. 4.

All non-hydrogen atoms were refined with anisotropic displacement parameters. All hydrogen atoms were placed in ideal positions and refined as riding atoms with individual isotropic displacement parameters. No solvent molecules were present in the structure. One butyl group of the TBA cation was found to be disordered. The major component of the disorder (60.1%) consists of atoms C18, C19, and C20. The minor component of the disorder (39.9%) consists of atoms C18', C19', and C20'. The anisotropic thermal parameters of atom pairs (C18, C18'), (C19, C19'), and (C20, C20') were constrained to be the same values. The distances between the atom pairs (C18, C19) and (C18', C19') were restrained to be equal within an effective standard deviation of 0.01. Likewise, the distances between the atom pairs (C19, C20) and (C19',

Table 1 X-ray Crystallographic Data for **2-o** and **2-c**

Structure	2-c	2-o
formula	C ₂₆ H ₄₇ N ₅ Pt	C ₂₆ H ₄₇ N ₅ Pt
color	colorless	orange
lattice type	monoclinic	triclinic
space group	P2 ₁ /c	P1-
a, Å	13.8830(11)	9.737(7)
b, Å	12.4658(10)	12.790(10)
c, Å	17.7056(15)	13.612(10)
α, deg	90	105.497(12)
β, deg	108.6250(10)	105.990(12)
γ, deg	90	109.101(12)
V, Å ³	2903.7(4)	1415.7(18)
Z	4	2
formula wt, g mol ⁻¹	624.78	624.78
D _c , g cm ⁻³	1.429	1.466
Temperature	223(2)	173(2)
μ, mm ⁻¹	4.853	4.976
F(000)	1264	632
reflns collected	23652	25251
unique reflns	6647	5037
data/restraints/parameters	6647 / 0 / 289	5037 / 3 / 260
R ₁ , wR ₂ (I > 2σ(I))	0.0284, 0.0609	0.0873, 0.2000
R ₁ , wR ₂ (all data)	0.0435, 0.0641	0.1111, 0.2108
goodness-of-fit	0.916	1.017

C20') were restrained to be equal within an effective standard deviation of 0.01. The bond lengths between atoms C18' C19' and C19' C20' were restrained to be the same values as those between atoms C18 C19 and C19 C20, respectively.

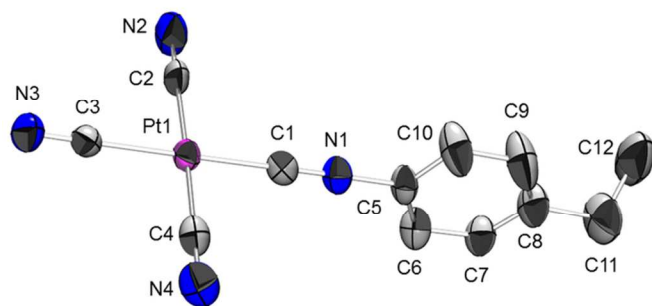


Fig. 4 Thermal ellipsoid diagram of the anion of (TBA)[Pt(CN)₃(CN-*p*-(C₂H₅)C₆H₄)] (**3**) (50% probability ellipsoids, cation and hydrogens omitted for clarity)

[Pt(TERPY)Cl][Pt(CN)₃(CNCH₃)] (**4**)

A crystal structure of **4** was not obtained after many attempts. The high insolubility of the salt limited recrystallization solvents. Immediate precipitation of **4** upon slow mixing or careful layering of even dilute immiscible solutions of the starting materials precluded crystal growth. Compound **4** has very limited solubility in DMF and DMSO.

Gravimetric Experiments

Hydration measurements were made with a custom built apparatus similar to the one previously described.⁹ A yellow bulk sample of **2** (no special drying conditions) at ambient humidity (0.1044g) was added to a preweighed foil cup and exposed to water saturated nitrogen vapor. After 24h, the mass had stabilized at 0.1066g and appeared white. The atmosphere of the sample chamber was then changed to dry nitrogen (<3% relative humidity) and the sample chamber was slowly heated using heat tape. The sample melted near 75°C and after 50 minutes of heating the mass stabilized at 0.1035 g. Upon cooling the measured mass remained the same, and the sample appeared orange. Using this final mass as the anhydrous sample mass, the amount of sample used was 0.166 mmol. The total moles of water picked up by the sample was equal to 0.17 mmol, or approximately one equivalent of water per mol of **2**.

A sample of **4** was added to a preweighed foil cup and exposed to water saturated nitrogen gas for 24h during which time it gained mass and came to an equilibrium mass value of 0.1228g. Mass readings were acquired while passing dry nitrogen gas through the heated sample chamber (>100°C) until the mass stabilized at 0.1108g. The measured mass remained at 0.1108 g upon cooling back to room temperature. Fig. 5 shows the mass loss as a function of time.

A similar set of mass values were recorded starting from a sample of **4** that was dried by heating under a nitrogen atmosphere then cooled to room temperature. The mass of the 'dry' sample (0.1117 g) was measured while water saturated nitrogen gas was supplied to the sample chamber. The mass increased until it stabilized at a final value of 0.1222g.

The amount of water sorbed by **4** can be calculated on a per mole basis using each of these mass experiments. Using the experiment where the mass of a 'dry' sample of **4** increased, the initial mass is taken as the anhydrous mass (0.1117 g, 0.145 mmol). The final mass of **4** indicates 4.0 (±0.5) moles of water per mole of double salt complex are sorbed. Using the experiment where the mass of a 'wet' sample of **4** decreased, the final mass is taken as the anhydrous mass (0.1108 g, 0.144 mmol). The final mass of **4** indicates 4.6 (±0.5) moles of water per mole of double salt complex are sorbed.

Powder X-ray Diffraction Data Collection

Room temperature (23°C) X-ray powder diffraction patterns were obtained with a Siemens D-5005 diffractometer with a 2.2 kW sealed copper source equipped with a single-crystal graphite monochromator, scintillation counter, and slits of [1°, 1°, 1°, 0.6°, 0.6°]. Powder diffraction patterns were collected from 2θ = 2-60° with a 2θ stepping angle of 0.02° and an angle dwell of 2 s. Variable-temperature X-ray powder diffraction scans were obtained on a Scintag XDS200 theta/theta diffractometer equipped with a high and low-temperature apparatus and slits of [1°, 2°, 0.5°, 0.3°] moving from the source to the detector. Patterns were collected in the step scanning mode from 2θ = 2-20° with a 2θ step angle of 0.02° and an angle dwell time of 2 s.

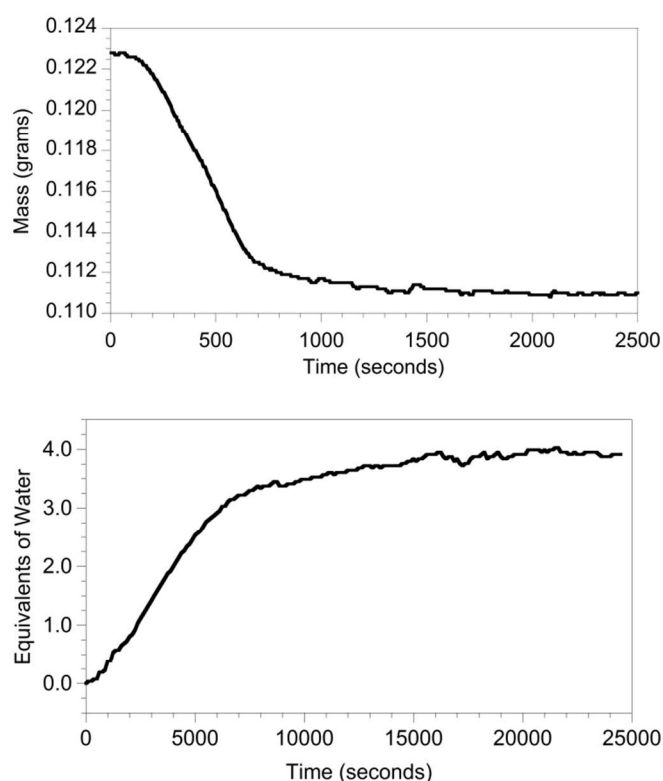


Figure 5 Gravimetric sorption studies of **4**. Graph of mass loss of solid **4** as dry nitrogen and heat were applied to the sample (above) and graph of mass uptake of solid **4** as the dry sample was exposed to water-saturated nitrogen vapour (below). Water uptake is shown in equivalents of water per mole of **4**.

The sample cell used was identical to the one previously described.⁹ Water vapor exposure of a room temperature solid sample of **2** was carried out by enclosing the sample holder in a small, resealable plastic bag. The powder patterns collected with the sample inside the plastic bag does not contain additional reflections in the $2\theta = 5\text{-}20^\circ$ data collection range. The sample was exposed to water vapor by placing glass wool saturated with 5 mL of water in the bag, which was then sealed to create a room-temperature atmosphere saturated with the water vapor. The sample, water vapor, and liquid water were allowed to come to equilibrium before a powder pattern was collected. X-ray powder patterns were also collected of **2** at -150°C and -190°C .

Simulated X-ray powder diffraction patterns were generated using the single-crystal unit cell as input (a PDB file generated from SHELXTL¹⁹) into the Cerius2 software program.²⁶ Lorentzian peak shapes were modeled. Simulation inputs were appropriate for the experimental pattern data collection conditions, including the X-ray source (Cu), wavelength (1.54178 Å), crystal monochromator (single), monochromator angle (13.288°), and monochromator spacing (3.3540 Å). Simulated powder patterns were constructed from low temperature single-crystal structural parameters (-100°C for **2-c**, -50°C for **2-o**), however experimental powder patterns were acquired at 23°C . A spreadsheet was constructed to fit the percentage of polymorph components in the experimental

powder pattern using the simulated powder patterns of the individual polymorphs **2-c** and **2-o**.

Attempts made to collect X-ray powder diffraction measurements of **4** resulted in very low intensity broad diffraction peaks. The quality of the data indicated the sample was poorly crystalline.

Infrared Water Exposure Study

A series of ATR-IR spectra were collected of **4** while water-saturated nitrogen vapor was exposed to the sample. The supplied stainless steel cover for the trough ATR cell was modified to form a sealed chamber above the ZnSe crystal sampling surface. Two holes were made through the cover and Luer ports were installed. The ports were used as inlet and outlet ports to supply the nitrogen gas to the sample. An o-ring between the cover and trough ATR cell formed an airtight seal. Water-saturated nitrogen gas was then saturated by slow bubbling through two bubblers filled with water.

Vapoluminescent Studies

Emission spectra were acquired as a function of time while a solid sample of compound **4** was exposed to water-saturated nitrogen vapor. The apparatus used to collect the vapoluminescent emission data is similar to that of a previously described previously system.⁸ The excitation source is a commercially available LED (Radio Shack) controlled using a variable voltage power supply. Though the light from the LED has a narrow wavelength range, an interference filter was used narrow the excitation profile to ≈ 5 nm. The excitation beam was brought to the sample via a bifurcated fiber optic with a stainless steel probe end in the sample chamber. The light collection branch of the bifurcated fiber optic was connected to an Ocean Optics CCD spectrometer. The solid sample is coated on a 100°C thermistor which protrudes from a hollowed out cylindrical Delrin plug (to accommodate the thermistor wires). The thermistor allows for flash heating of the sample prior to a water exposure to remove any residual water and begin an experiment with a totally dry sample. A solid Delrin sample holder with no thermistor is used when heat is unnecessary to dry the sample.

Statistical Treatment of Vapoluminescent Emission Data

A series of solid-state emission spectra were collected at known time intervals while a sample of **4** was exposed to water-saturated nitrogen gas. The data set acquired shows a complicated series of changes not easily explained by an A \rightarrow B transformation. In theory, a fitting routine could be used where a kinetic scheme is proposed and then epsilon values for multiple species are fit at every wavelength as a function of time. In practice this is computationally unwieldy. Principal component analysis (PCA) was used to identify the number of species present in this data series and the spectrum of each component. PCA is a mathematical treatment that allows multiple correlated variables to be explained more simply. The goal is to represent the variation present in many variables into a few principal components.²⁷ Each principal component is

exhibits an axial chair conformation. The isocyanide bond angle of C1-N1-C5 is significantly less than linear ($170.9(4)^\circ$). No close intermolecular Pt-Pt contacts are present. The shortest Pt-Pt distance is 8.407 \AA between two anions oriented with their square planes in the same plane.

The PLATON/SQUEEZE programs²⁸ were used to identify possible disordered or partially occupied solvent molecules in the structure of **2-c**. The results from SQUEEZE indicated there were 4 possible voids per unit cell. They are found as 2 pairs with coordinates averaged over special positions. The fractional coordinates of the 4 sites are (0.482, -0.033, 0.570), (0.519, -0.036, 0.425), (0.518, 0.467, 0.930), and (0.481, 0.536, 0.075). The first two are very close to (0.5, 0, 0.5) and the second pair are very close to (0.5, 0.5, 0). These special positions in $P2_1/c$ have inversion site symmetry. The pairs of solvent accessible sites have volumes of 35 \AA^3 per each pair. This is an acceptable volume for a water molecule (volume of about 22 \AA^3). It is also possible that the voids are only partially occupied by water. The void locations are in a region close to the nitrile nitrogen. The voids were found to occupy 70 \AA^3 , or 2.4% of the total unit cell volume. A total electron count of 6 electrons (less than one water molecule) was found in the voids.

The structure of **2-o** (Figure 3) is very similar to **2-c**, but shows important differences upon close inspection. The cyclohexylisocyanide exhibits an axial chair conformation. Close intermolecular distances between the cyclohexylisocyanide groups of two adjacent anions are present. The distances between atom N1 of one anion and C5 and C10 of the neighboring anion are only 3.527 \AA and 3.457 \AA , respectively. As the closest monoanion pairs shown in Fig. 3 are related by inversion, a second set of these contacts are present as well. Another interesting feature is the bond angle of C1-N1-C5 which is $175.5(14)^\circ$. No close intermolecular Pt-Pt contacts (shortest Pt-Pt distance 7.484 \AA) are present. A structural overlay and detailed comparison of the structures of **2-o** and **2-c** are shown in Figure 6.

PLATON/SQUEEZE was also used to identify possible voids in the structure of **2-o**. The results from SQUEEZE indicated there are 2 possible voids in the structure per unit cell. The fractional coordinates of the two void sites are (0.331, 0.138, 0.936) and (0.669, 0.861, 0.064). They are found as a pair with coordinates averaged over the special position (0.5, 0, 0). This special position has inversion site symmetry. The combined volume of these two voids is 34 \AA^3 and the total electron count found in the voids was 4 electrons per unit cell. Again, this volume is acceptable for a water molecule but the electron density is insufficient to account for the presence of even one water molecule in the void.

Figure 4 shows the square planar structure of **3**. The bond lengths and angles are representative. No significant stacking interactions were found between platinum atoms. The closest Pt-Pt distance in the structure is 8.618 \AA . A π -stacking dimer interaction between the phenyl groups of two anions was found, shown in Figure S2. The π -stacking interaction is limited to discrete dimer units. The distance between the least-squares

planes composed of the phenyl group carbon atoms of the paired anions is 3.808 \AA .

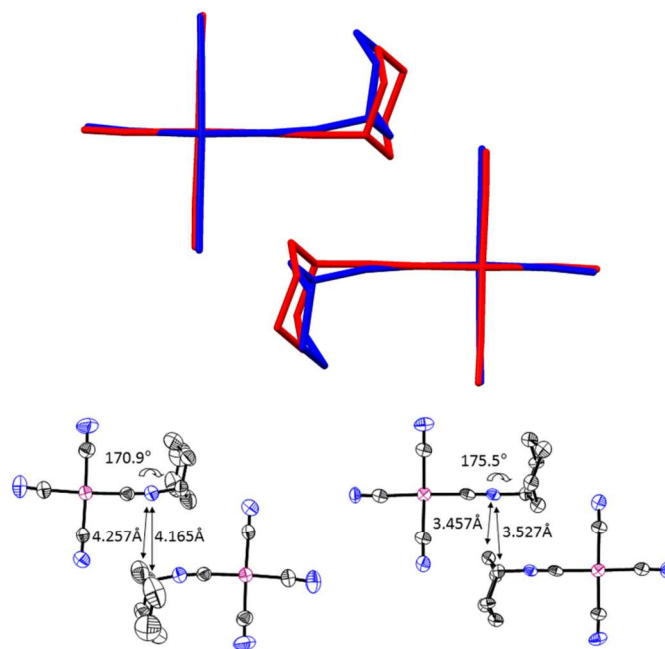


Fig. 6 Overlay of the crystal structures of **2-o** (red) and **2-c** (blue) (above, cations omitted) and comparison of bond angles and close intermolecular approach of **2-o** and **2-c** (below, cations omitted).

X-ray Powder Diffraction

The phase behavior of compound **2** was studied using X-ray powder diffraction. The isolation of a bulk sample of yellow powder of **2**, followed by the growth of a colorless crystal of **2** (**2-c**) prompted further study. The powder diffraction pattern of a bulk powder sample of **2** at room temperature is (Fig. 7A) is very complicated. A theoretical powder pattern of **2-c** was then generated using the single-crystal structure. Peaks from the simulated pattern of **2-c** accounted for some of the peaks in the bulk yellow sample powder pattern of **2** but not all (Fig. 7C). A theoretical powder pattern of **2-o** was then generated using the single-crystal structure (Fig. 7D) and compared with the remaining peaks in the experimental powder pattern of bulk yellow **2**. The identity of **2** is confirmed to be a mixture of two crystalline polymorphs **2-c** and **2-o**. A linear combination of simulated powder patterns of polymorphs **2-c** and **2-o** was fit to the experimental pattern collected (Fig. 7B).

The calculated amount of each polymorph in the experimental pattern is 85.3% **2-c** and 14.7% **2-o**. The experimental powder pattern was assumed to contain only contributions from polymorphs **2-c** and **2-o**. The agreement of the simulation with the experimental data suggests this is a reasonable assumption. The slight shift in position of all peaks from simulated patterns relative to the peaks from the experimental pattern can be explained as a temperature effect. Simulated pattern peaks were generated from low temperature data (-100°C or -50°C), which likely show contraction of the unit cell parameters relative to the experimental data collected

at 23°C. Low temperature powder patterns collected at -150°C and -190°C did not modify the polymorph ratio of **2-c**/**2-o** in a bulk yellow sample of **2** (Figure S3). The d-spacings of peaks in the entire pattern increase slightly as expected for contraction of the unit cell at low temperature.

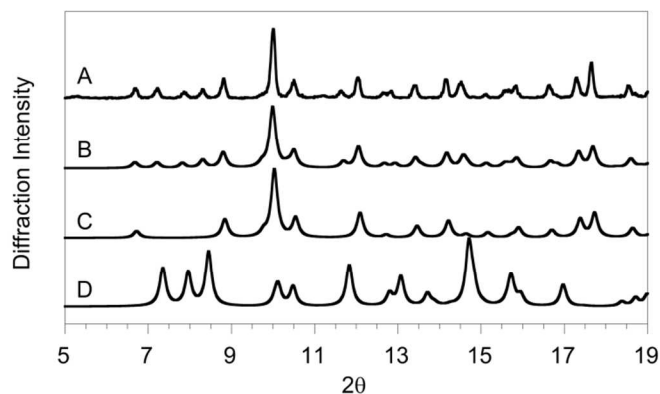


Fig. 7 Experimental X-ray powder diffraction of a bulk sample of **2** at ambient humidity (A), a composite simulation of 85% **2-c**/ 15% **2-o** from powder patterns generated from single-crystal structure data (B), simulated powder pattern generated from single-crystal structure **2-c** (C), and the simulated powder pattern generated from single-crystal structure **2-o** (D).

Once the polymorphic composition of a bulk sample of **2** was elucidated, additional powder diffraction studies were performed to determine if **2** was vapoluminescent. The X-ray powder diffraction pattern was acquired of a bulk sample of **2** (yellow in appearance) at ambient humidity. The sample was then exposed to 95% humidity for a period of 24 h in a sealed plastic bag. The powder diffraction pattern of **2** (now white in appearance) was obtained while in the plastic bag. The comparison of the 95% humidity experimental powder pattern with the ambient humidity experimental pattern and the calculated powder pattern from the structure of **2-c** are shown in Figure 8.

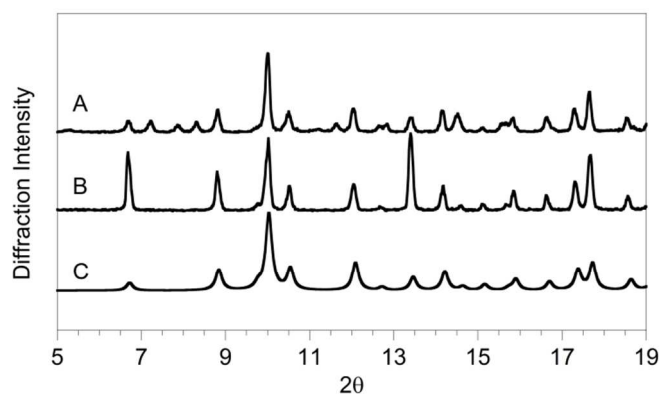


Fig. 8 Experimental X-ray powder diffraction of a bulk sample of **2** at ambient humidity (A), exposed to 95% humidity (B), and the simulated powder pattern generated from single-crystal structure **2-c** (C).

The ambient humidity pattern is consistent with the mixture of colorless (**2-c**) and orange (**2-o**) polymorphs. The 95% humidity powder pattern however is consistent with the

presence of only the colorless polymorph (**2-c**). The intensities of the peaks in the 95% humidity powder pattern are not identical to those of the calculated pattern. The intensity differences observed between these patterns could be explained by possible preferential orientation of the crystallites in the sample holder relative to the diffraction geometry. Intensities calculated for the pattern of **2-c** assume no preferential ordering of the sample crystallites. Our work with the X-ray powder diffraction of other square-planar platinum compounds have shown that preferential orientation frequently occurs with these types of molecules.⁵

Infrared Spectroscopy

The infrared spectra of complexes **1-3** are consistent with the predicted C_{2v} symmetry of the monoanions. The infrared absorptions in the 2210-2260 cm^{-1} region are assigned as coordinated isocyanide stretches. Absorptions in the 2135-2160 cm^{-1} region are assigned as coordinated cyanide stretches. A comparison of the infrared spectra of complexes **1-3** (Figure 9) shows how the substituent of the isocyanide effects the isocyanide stretching frequency, but negligible differences are observed in the cyanide stretching frequencies. As the electron donating ability of the isocyanide substituent increases, the π -accepting ability of the isocyanide decreases, and thus the stretching frequency observed decreases ($R = p\text{-}(\text{C}_2\text{H}_5)\text{-C}_6\text{H}_4 < c\text{-C}_6\text{H}_{11} < \text{CH}_3$).

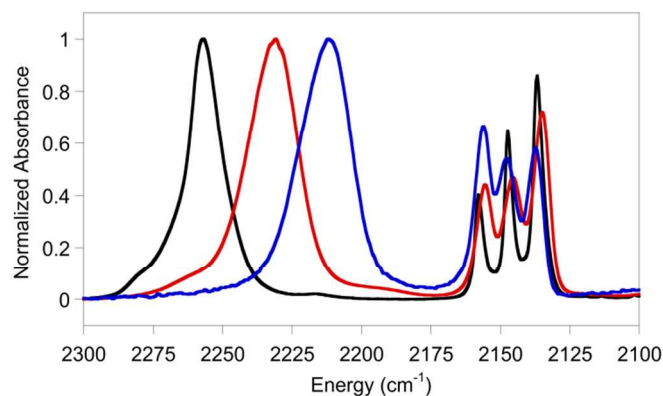


Fig. 9 Normalized solid-state ATR-IR spectra of **1** (black), **2** (red), and **3** (blue).

Differences in the infrared spectra of **4** and **1** show interesting changes in the environment of the $[\text{Pt}(\text{CN})_3(\text{CNCH}_3)]^-$ anion. While the cyanide stretches at 2157 and 2148 cm^{-1} for **4** are quite similar to those at 2158 and 2147 cm^{-1} for **1**, the lowest energy cyanide stretch and the isocyanide stretch show significant differences. Changing the cation from TBA^+ to $[\text{Pt}(\text{terpy})\text{Cl}]^+$, the cyanide stretch at 2137 cm^{-1} (**1**) decreases to 2131 cm^{-1} (**4**), while the isocyanide stretch at 2257 cm^{-1} (**1**) increases to 2267 cm^{-1} (**4**) (Figure S4). These changes suggest that the isocyanide ligand in the $[\text{Pt}(\text{CN})_3(\text{CNCH}_3)]^-$ anion of **4** experiences less π -backbonding while a cyanide ligand or combination of cyanide ligands of the anion experiences more π -backbonding compared with **1**. Since the same platinum orbitals that mediate π -backbonding to the

isocyanide ligand also do the same for the *trans* cyanide ligand, the difference in the stretching frequencies between the **1** and **4** can be explained as a net shift in the anion dipole. The cause of this shift is likely the close proximity of the planar [Pt(terpy)Cl]⁺ cation which also has a dipole and could provide a Pt-Pt interaction to stabilize the close association of these ions in the solid-state.

ATR-IR spectra were also collected of **4** as the sample was exposed to water-saturated nitrogen vapor. Figure 10 shows the response of **4** as a function of time with exposure to 95% rh. Significant changes are evident in the cyanide stretching frequencies of the monoanion (2120-2170 cm⁻¹). All the cyanide stretches shift to higher energy upon exposure to water. This is consistent with less Pt π -backbonding to the cyanide ligands and a strengthening of the cyanide triple bonds. These changes are likely the result of hydrogen-bonding of the nitrile lone pairs with water molecules that have entered the crystal lattice. More subtle changes are seen in the isocyanide band. These could be inductive effects caused by changes in the cyanide ligands. Purging the sample with dry nitrogen gas after this water exposure results in a complete return to the original spectrum. The interaction of water molecules with the cyanide ligands of the anion of **4** is clear.

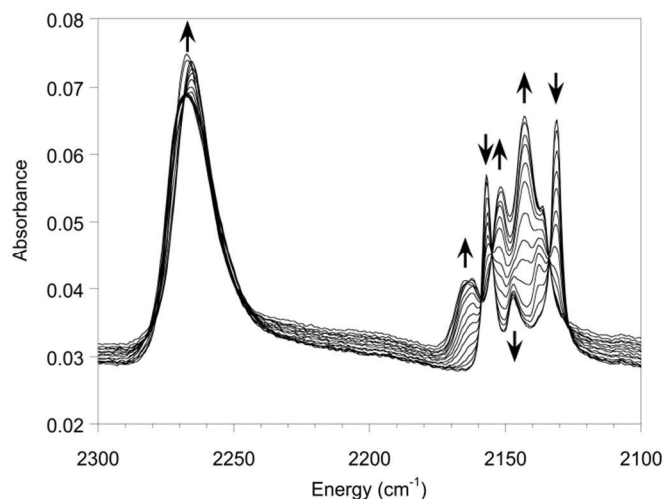


Fig. 10 ATR-IR spectra of solid **4** exposed to water-saturated nitrogen vapor. Arrows indicate changes relative to the initial spectrum of a dry sample of **4**.

This is consistent with previous studies in our group which showed that hydrogen bonding solvents elicit cyanide stretching frequency changes with accompanying vapoluminescent changes in the visible or NIR regions.⁴

UV-Vis Absorption

Solution UV-Vis absorbance spectra of the monoanions were collected in the range of 250-600 nm. The observed peaks are consistent with high energy MLCT bands due to their large absorptivity values. These MLCT bands are tentatively assigned as Pt(d) \rightarrow $\pi^*(\text{CN}, \text{CNR})$ transitions. Monoanion **3** shows slightly lower energy absorption bands relative to **1** and **2** as the phenyl isocyanide is more electron rich, stabilizing the

π^* orbitals. None of the anions have any absorption bands in the visible region in solution.

Solid-state UV-Vis spectra were acquired for compound **4**. Figure 11 shows the UV-Vis spectrum of **4** in a dry nitrogen atmosphere (<3% rh) and in the presence of water saturated nitrogen vapor (95%rh). The 'dry' spectrum is regenerated by exposing the film of **4** to a 'dry' nitrogen stream again. The 'dry' spectrum of **4** has absorption bands at 556 nm and 479 nm and the sample appears purple by eye. The high humidity spectrum of **4** has absorption features at 490 nm and 468 nm and the sample appears orange to the eye. These strong absorption features in the visible region are likely due to a MMLCT transition which arises from a Pt-Pt interaction. The interaction may be between a monocation and monoanion in a linear chain stack as similar dication/dianion structures show.^{5,9}

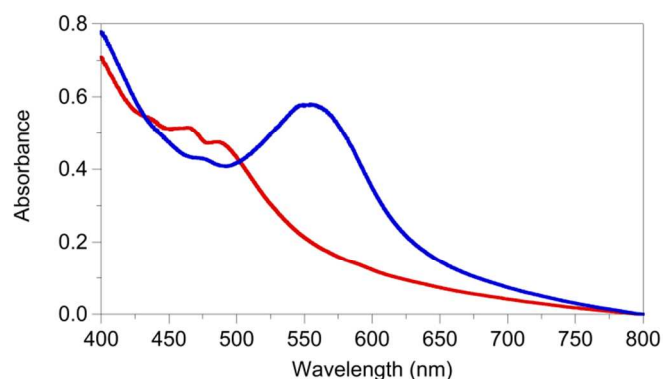


Fig. 11 Solid-state UV-Vis spectra of **4** collected in a 95% rh atmosphere (blue) and in a 5% rh atmosphere (red).

Emission

The room temperature low energy emission bands present in the spectra of solid samples of **1**, **2**, and **3** were surprising. The solid emission spectrum of a film cast from an acetone solution **1** is shown in Figure S5. The single emission band of **1** at 497 nm is unlike the related compound (TBA)₂[Pt(CN)₄] which does not emit under identical conditions. The emission spectrum of a solid crystalline sample of **3** is shown in Figure S6. The emission bands of crystalline **3** (592 nm, 645 nm) are much lower in energy than the film of **1** and vibronic structure is present. The difference in the energy of the emission bands of **3** (\approx 1400 cm⁻¹) is consistent with an excited state distortion involving a phenyl ring vibration. An acetone solution cast film of **3** showed no emission under the same conditions.

Solid emission spectra of compound **2** were highly dependent on the preparation and environment of the sample. The emission spectrum of a bulk solid sample of **2** (yellow in appearance) taken at 15% rh has an emission band at 542 nm. Upon exposure to 95% rh for 15 min, the intensity increases to 266% of its original value, but the λ_{max} remains unchanged. However if the sample continues to be exposed to 95% rh for 6h, the emission intensity eventually decreases to 16% of its original value and now appears white. This series of spectra are shown in Figure 12.

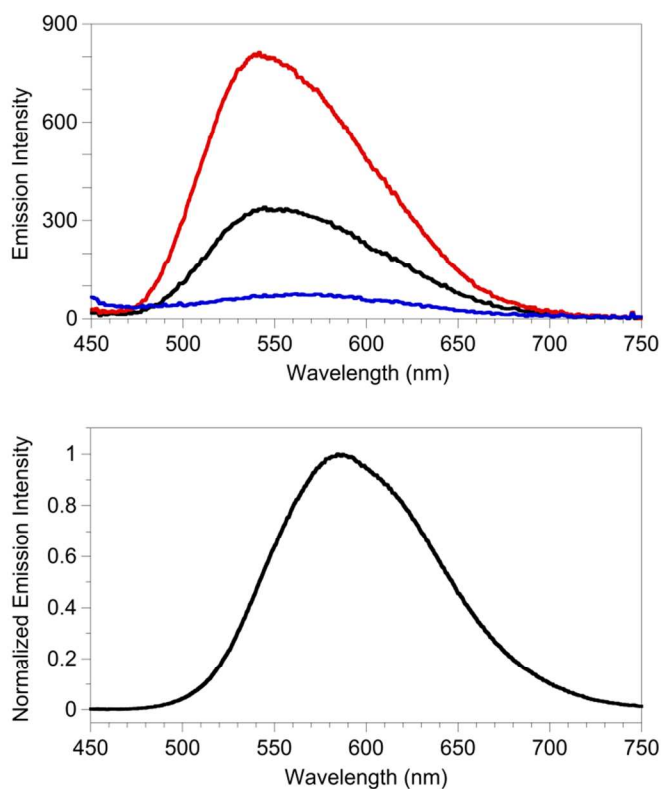


Fig. 12 Uncorrected solid-state emission spectra of a bulk sample of **2** at 15% rh (—), exposure to 95% rh for 15 min (—○—), and exposure to 95% rh for 6 h (—△—) (above); Solid-state emission spectrum of a bulk sample of **2** melted and solidified under <3% rh (below).

Additionally, if the bulk yellow solid is melted (60°C), cooled to rt and allowed several weeks to resolidify under a dry atmosphere (<3% rh), an orange solid is obtained which has an emission band maximum at 587 nm, as shown in Figure 12. The emission band of this orange solid is at lower energy than the bulk yellow sample. Exposure of this orange solid to water produces an emission spectrum with a band at 542 nm, just as the bulk yellow sample at 15% rh.

The emission spectrum of a solid sample of **4** was found to be very sensitive to the humidity of the environment surrounding the sample. Solid-state emission spectra were collected of **4** under three different humidity levels as shown in Figure 13. At low humidity (<3% rh) the emission spectrum has a band at 670 nm. Upon exposure to 9.5% rh, the emission has the same energy but the intensity is 133% of the lowest humidity spectrum. The emission spectrum of **4** exposed to 95% rh shows a dramatic shift to lower energy ($\lambda_{\text{max}} = 708$ nm) and the intensity is 74% of the lowest humidity spectrum. These static humidity solid-state emission data for **4** are corrected for grating efficiency and detector response.

A series of solid-state emission spectra of **4** were collected starting from a dry sample exposed to 95% rh. Figure S7 shows some of the spectra collected during the time series acquisition. The entire data collection (the complete conversion from dry to fully hydrated) lasted 4 s and data were collected every 50 ms.

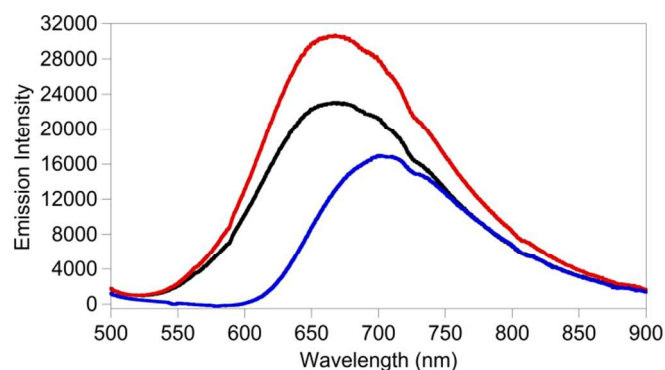


Fig. 13 Corrected solid-state emission spectra of **4** exposed to nitrogen gas of various relative humidities; <3% rh (black), 9.5% rh (red), and 95% rh (blue).

While data for the vapoluminescent changes were acquired over a span of 4 s, the total change from dry to fully hydrated was complete in ca 2.0 s. The spectra shown were collected approximately 200 ms apart. The same trend is shown in the time series collection as the emission spectra taken at static humidity levels. Initially, the emission band increases in intensity without shifting in energy, then later in a second process the emission band intensity decreases below the level of the initial spectrum and also shifts to lower energy. The spectra of this time series acquisition were not corrected for grating efficiency and detector response. A similar set of experiments involving the reverse process (replacing 95% RH with dry nitrogen (<3% RH)) yielded results with a similar time observed to return to the dry emission spectrum.

PCA Analysis of Vapoluminescent Data

Based on qualitative observation of the emission data, the presence of an intermediate which appears and diminishes through the vapor exposure, a beginning model based on Reaction 2 was used.



This Reaction 2 scheme assumes only that a chromophore responsible for phase A converts to phase B, and phase B converts to a third phase C. This scheme is reasonable based on the observation that other vapochromic platinum materials exhibit multiple solvates upon vapor uptake.^{5,9} These solvates can be treated as individual polymorphs. The kinetic equations used for this solid-solid phase transformation were modeled after those of Prout et al.²⁹ The kinetic model of the solid-solid transformations used by Prout et al has been used to analyze of solid-solid phase transformations in complex pharmaceutical polymorphic systems³⁰ and by our group in the analysis of vapoluminescent materials.¹⁰

The signature reaction profiles of solid-solid transformations are sigmoidal in shape. These transformations typically involve a reaction course with three periods; an 'induction' period, an 'acceleratory' period, and a 'decay' period.^{29,31} In an A→B transformation, the induction period is described as the formation of nuclei of B at the surface cracks

or strain lines of A. The acceleratory period is viewed as three-dimensional growth of the nuclei early in the transformation when many locations for transformation are accessible. The decay period shows a slowing down of the transformation as the sites for crystal growth are few. The kinetic expression shown as Equation 3 adequately describes the sigmoidal reaction profile of these solid-solid phase transformations.

$$e^{-k(t-t_{1/2})} = x / (1-x) \quad (3)$$

In Equation 3, t is the time, $t_{1/2}$ is the time required for 50% conversion, and x is the mole fraction of B at time t . This equation was extended algebraically to an $A \rightarrow B \rightarrow C$ scheme for modeling the vapoluminescent response of **4**.

Using PCA on the luminescent data of **4** exposed to 95% rh, two principal components captured most of the variance in all the data. PC1 accounted for 93.3% of the variance while PC2 accounted for 5.6%, for a total of 98.9% total variance in all the data captured between these two PCs. The magnitude of PC1 was used to model a proposed kinetic scheme and is plotted in Fig. 14.

Attempts to model the changes in the emission data with only two species ($A \rightarrow B$) gave a poor fit to the PCA vs time data. However, a fit with three species ($A \rightarrow B \rightarrow C$) modeled the PCA vs time data well. The spectral changes of three species, each with an epsilon value for its relative contribution to the intensity at PC1, a rate constant k_1 and a time lag parameter t_1 for $A \rightarrow B$, and k_2 and t_2 for $B \rightarrow C$ were used to model the PC1 vs time plot. These parameters were fit to PC1 using a nonlinear least-squares fitting routine. Figure 14 shows the score of PC1 vs time and the kinetic model fit for the $A \rightarrow B \rightarrow C$ mechanism.

The kinetic fit parameters were as follows: $k_1 = 15.3865$, $t_1 = 1.50946$, $k_2 = 5.36896$, $t_2 = 1.87522$, $\epsilon_a = 293.2031$, $\epsilon_b = 1049.02$, $\epsilon_c = -401.041$. These epsilon values are in PC1 space which is mean centered so the negative values of ϵ are reasonable. Using the kinetic fit parameters, calculated emission spectra of each phase were generated (Fig. 14). The results of the kinetic fit with PC1 were then used to produce concentration profiles of the species as a function of the time course of the emission changes (Fig. 15). The reverse process experiments (replacing 95% RH with dry nitrogen (<3% RH)) were not modeled using PCA.

Discussion

Polymorphs of Compound 2

The motivation to understand the curious behavior of compound **2** came from the large color difference between the yellow bulk sample obtained, the first crystal structure of colorless **2-c**, and later the orange **2-o**. Only subtle structural differences are present between **2-c** and **2-o**, and yet methylene chloride solutions of both **2-c** and **2-o** appear colorless and have the same ^1H NMR spectrum.

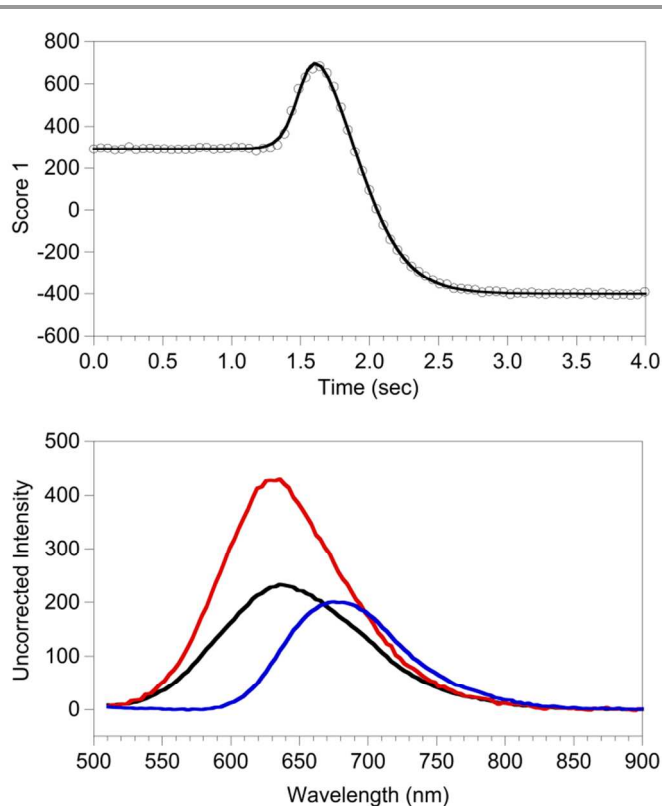


Fig. 14 A plot of score 1 vs time for the PCA analysis of the solid emission spectra of **4** collected during exposure to 95% rh; score data points (o), fit to the kinetic model (—) (above) and calculated solid emission spectra from PCA analysis of **4**; species A (—), B (—), and C (—) (below).

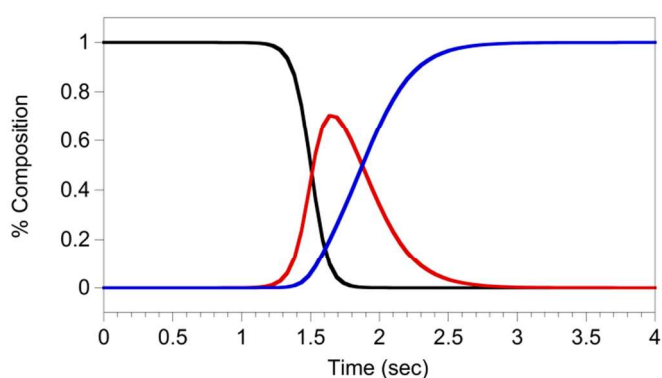


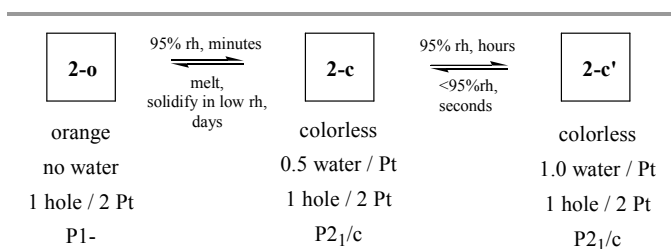
Fig. 15 PCA calculated concentration profiles of emitting species A (black), B (red), and C (blue) as a function of time for exposure of **4** to water-saturated nitrogen vapor.

Thus the color evident in the solid-state of **2-o** must arise from intermolecular interactions, of which only close π - π interactions of isocyanide ligands are present (Fig. 5). Though the closest isocyanide distances are beyond van der Waals contact (N1-C5 3.527 Å, length - vdW radii sum = + 0.277 Å), even a small ground state intermolecular interaction between the isocyanide orbitals could have significant consequences. Another possibility is an excited-state distortion that involves a closer approach than observed in the ground-state geometry. For the isolated anion (as in **2-c** or in solution) the lowest

energy feature in the absorbance spectrum is assigned as a MLCT transition from a primarily Pt-based filled d orbital to an empty π^* orbital of the isocyanide. As isocyanide ligands begin to interact as their intermolecular distance decreases, an additional splitting of the π^* orbitals would give rise to a new lower energy LUMO. This is the most likely possibility based on the data at hand.

The role that water plays in the polymorphic behavior of **2** was also investigated. Water vapor-induced interconversion of **2-c** and **2-o** was demonstrated by powder diffraction. Gravimetric experiments showed concomitant mass gain during polymorph conversion. The gravimetric data indicated the net loss of one mole equivalent of water per mole of **2**, consistent with the X-ray powder diffraction and the combustion analysis which indicated approximately one mole of water per mole **2**. However, no water molecule was found in the structure of **2-c**. Application of SQUEEZE to **2-c** indicated voids of appropriate size for water were present but insufficient electron density to account for full occupancy by water. The void positions are however close enough to enable hydrogen-bonding with the nitrile nitrogen N2 for any possible water present. It is likely that either no water is present in the collected X-ray structure of **2-c** or that water molecules partially occupy these holes and are positionally disordered. Using SQUEEZE on the orange morph **2-o**, one void of appropriate size for one water molecule was found per unit cell but with insufficient electron density for full occupancy.

A model which takes into account the powder and single crystal X-ray results of **2** as well as the balance experiments is summarized in Scheme 2.



Scheme 2 Model describing the polymorphs of **2**.

Structure **2-o** contains no water while the colorless morph X-ray structure **2-c** collected contains some water (\approx 0.5 molar equivalent per anion). An additional proposed polymorph **2-c'**, with one full equivalent of water per anion, is implicated during balance experiments, where water is absorbed, and in the X-ray powder pattern of the high humidity exposure of **2**. The fully hydrated morph **2-c'**, assigned as the high humidity powder pattern, has very similar peak positions relative to **2-c** (similar proposed unit cell to that of **2-c**) but the unit cell contents shift slightly. The voids in the structure of **2-c** are already larger than necessary for one water and small changes in the alkyl chain positions of the TBA⁺ cation can readily expand the void size to accommodate two water molecules per void or one molar equivalent of water per mole of anion. The relative kinetic processes that govern the interconversion of the polymorphs are also indicated in the model. To completely

remove water from **2-c**, heat or a long time period without heat is necessary to convert **2-c** to **2-o**. Exposure of a sample that is primarily **2-o** to water vapor takes less time to convert back to **2-c** than from **2-c** to **2-o**, but the **2-c** to **2-o** conversion is also slow. Less is understood regarding the interconversion of the **2-c** and **2-c'** polymorphs, which have different hydration levels. The volume of the voids in both **2-c** and **2-o** are most consistent with occupation by only one water molecule if they are filled.

The changes seen in the emission spectra of solid samples of **2** are less consistent with this proposed model of polymorphs. The emission intensity of a bulk sample of **2** essentially disappears as the presence of **2-o** is completely diminished upon exposure to high humidity for enough time to fully hydrate. The fact that the emission peak maximum of the bulk sample of **2** is not the same as that of the fully hydrated morph (no emission) or that of **2-o** is puzzling. The changes in the emission spectrum of solid **2** induced by exposure to water vapor allows classification of this compound as vapoluminescent. The slow kinetics of the changes observed in the emission spectra however prohibit this compound from practical use as a humidity sensor.

Emission Properties

Close examination of the structural features of each anion revealed a different origin of a low energy excited state for each anion, none of which include a significant Pt-Pt interaction. The structure of **1** reveals close interactions between the lone pairs on nitrile nitrogens with the hydrogen atoms of the methyl isocyanide. Each monoanion participates as both a nonclassical hydrogen-bond donor and acceptor using the mutually *trans* cyanide and isocyanide ligands. The close isocyanide-isocyanide approach in the structure of **2-o** allows pairwise intermolecular interactions between monoanions. The structure of **3** shows a close π - π interaction of the phenyl groups of the isocyanide ligands of pairs of monoanions. It is postulated that in the solid-state, each monoanion has a low energy excited state present because an intermolecular phenomena couples the chromophores of at least two monoanions. The origin of the emitting excited state in each case is tentatively assigned as originating from a ³(MLCT) state that involves a new ligand π^* orbital that arises from an intermolecular interaction.

The excited state origin of the emission of **4** is less clear, in part because the structure is not available. The emission does not originate from a terpy ligand localized ³($\pi^* \rightarrow \pi$) transition as the energy of the emission band of **4** is too low for that type of excited state. The emission of cold dilute solutions of [Pt(terpy)Cl]⁺ where chromophores are assumed to be monomeric in nature appears at 470nm.³² The low energy emission band of **4** is likely the result of a MMLCT ($d \pi^*(Pt_2) \rightarrow ^3(\pi^*(terpy))$) (metal-metal-to-ligand charge transfer) transition where a close metal-metal interaction is present in the structure. This assignment is consistent with the assignment of solid emission spectra of various [Pt(terpy)Cl]⁺ salts with noncoordinating anions and with other vapoluminescent double salt compounds of the forms [Pt(CNR)₄][Pt(CN)₄] and *cis*-[Pt(CN)₂(CNR)₂]. Recent TDDFT calculations performed on

the vapoluminescent salt [Pt(terpy)Cl](PF₆) support the significance of Pt...Pt (and π - π) interactions in modulating the electronic structure of these types of stacking structures.³³

Structure of 4

A Pt-Pt interaction and/or π - π interaction is likely in the structure of **4** based on the low energy absorption and emission bands but direct evidence of these interactions is not available. One question to pose regarding the structure of **4** is whether the cation and anion alternate within the same stack (heterosoric stacks), cations and anions stack in separate stacks (homosoric), or whether one ion (either cation or anion) stacks while the other fills voids without any stacking interactions. Currently, there are no crystallographic examples of [Pt(terpy)Cl]⁺ double salts with square planar Pt(II) containing anions that stack in alternating cation/anion linear chain type structures. However, a few related examples are reported with planar Au(I) anions including [Pt(terpy)Cl][Au(CN)₂],³⁴ [Pt(terpy)Cl][AuCl₂],³⁴ and [Pt(terpy)Cl][Au(C₆F₅)₂]³⁵ that stack with cation/anion interactions with short Pt...Au distances.

Vapoluminescent Behavior of 4

Compound **4** is the first example of a new class of vapoluminescent materials, namely a monoanion/monocation platinum double salt complex. While **4** responds to water vapor, other [Pt(terpy)Cl]⁺ (or related cation) salts of noncoordinating anions have been reported to exhibit vapoluminescence. For example, [Pt(terpy)Cl](PF₆) is vapoluminescent in response to acetonitrile.³³ The salt [Pt(Cl-4-terpy)Cl]Cl demonstrates vapoluminescent behavior in response to methanol.³⁶ The related vapoluminescent complex [Pt(Me₂bzimpy)Cl](PF₆) (Me₂bzimpy = 2,6-bis(1-methylbenzimidazol-2-yl)pyridine) which has a NNN tridentate ligand similar to terpy, responds to acetonitrile.³⁷

The behavior of **4** was examined by various methods to understand the mechanistic details of the vapoluminescence. Mass experiments confirmed that four water molecules per mole of **4** were incorporated into the crystalline lattice. Previous studies indicate that the molar equivalent quantities of solvent sorbed by these types of materials are limited by the crystallographic restraints of symmetry to integer values related to the pure crystalline phases of the material. Examination of the experimental mass pickup or loss graphs (Figure 5) show no significant buildup of intermediates based on the relatively smooth curvature of the data.

Infrared spectroscopy of solid **4** exposed to water vapor shows significant changes in the cyanide stretching frequencies. This is consistent with water molecules hydrogen-bonding with cyanide ligands of the anion in the solid-state. Changes in the solid-state absorbance of **4** indicate small changes at low humidities and large changes at higher humidities. Static humidity solid-state emission spectra of **4** show the same type of behavior, where at low humidities mostly intensity changes occur while at higher humidities the intensity and energy of the emission band changes.

PCA analysis of a series of data demonstrating the intermediate species between low and high humidity exposure. The 'pure' spectra of each component (A, B, and C) concentration profiles and are displayed in Figures 14 and 15. As the static humidity emission spectra demonstrate, the vapoluminescent series of data collected indicate a phase or hydrate that exists only under certain conditions. This species B is likely the dihydrate complex of **4**. Though the evidence to support this species is not present in the mass pickup data, a theoretical mass increase graph was constructed from the concentration profiles found in the PCA analysis of the emission data (Figure S8).

The presence of all three species in significant proportions during most of the mass pickup blurs the expected inflection point caused by the intermediate species even in this simulation. The time scale necessary to fully hydrate a 100 mg sample in the mass pickup experiment is also much longer than the emission experiment which employs a high surface area thin sample film so it is reasonable there is no evidence of the partial hydrate B in the mass experiment. One possible explanation for the emission intensity increase of B relative to A is that the certain non-radiative energy dispersive pathways are shut down upon exposure to low humidities where hydrogen-bonding takes place but does not cause large structural changes.

Compound **4** has excellent potential as a vapoluminescent sensor material for water. The fast, reversible, wavelength and intensity changes in the emission spectrum are favorable qualities for practical sensor applications. Compound **4** does not possess the intended enhanced solubility relative to previously reported dication/dianion double salts of the type [Pt(CNR)₄][Pt(CN)₄]. Judicious choice of solubilizing pendant alkyl groups on the terpy ligand of the cation could enhance solubility for structural characterization and processing purposes.

Conclusions

A new class of square planar Pt(II) monoanions with one isocyanide and three cyanide ligands have been synthesized and characterized. These emissive monoanions exhibit interesting intermolecular interactions in the solid-state as shown in their X-ray crystal structures. The monoanion **2** exhibits different polymorphs, one of which has pairwise intermolecular isocyanide π - π interactions giving rise to a low energy emission band. Complex **2** is also the first Pt(II) vapoluminescent material composed of a non-coordinating salt of a monoanion. Another new type of vapoluminescent material was prepared as a monocation/monoanion double salt complex **4** was made using a novel monoanion. Mechanistic studies of this sensor material indicate that water molecules enter the solid material and undergo hydrogen-bonding interactions with the cyanide ligands of the monoanion. Three phases of **4** are also accessible; an anhydrous form, a partial hydrate, and a tetrahydrate. PCA of a set of emission spectra acquired during

an exposure of 4 to water vapor allowed spectra to be extracted of each of the three polymorphs.

Acknowledgements

The authors acknowledge Dr. Victor G. Young Jr. and Dr. William Brennessel of the University of Minnesota X-ray crystallography laboratory for assistance with the crystal structures.

Notes and references

- O.S. Wenger, *Chem. Rev.*, 2013, **113**, 3686; C. Jobbagy and A. Deak, *Eur. J. Inorg. Chem.* 2014, **27**, 4434; Kobayashi, Atsushi; M. Kato, *Eur. J. Inorg. Chem.* 2014, **27**, 4469; X. Zhang, B. Li, Z.-H. Chen, and Z.-N. Chen, *J. Mater. Chem.* 2012, **22**(23), 11427.
- C.L. Exstrom, J.R. Sowa Jr., C.A. Daws, D.E. Janzen, K.R. Mann, G.A. Moore, and F.F. Stewart, *Chem. Mater.*, 1995, **7**(1), 15.
- C.A. Daws, C.L. Exstrom, J.R. Sowa Jr., and K.R. Mann, *Chem. Mater.*, 1997, **9**(1), 363.
- C.L. Exstrom, M.K. Pomije, and K.R. Mann, *Chem. Mater.*, 1998, **10**(3), 942.
- C.E. Buss, C.E. Anderson, M.K. Pomije, C.M. Lutz, D. Britton, and K.R. Mann, *J. Am. Chem. Soc.*, 1998, **120**, 7783.
- S.M. Drew, D.E. Janzen, and K.R. Mann, *Anal. Chem.*, 2002, **21**(5), 993.
- J.W. Grate, L.K. Moore, D.E. Janzen, D.J. Veltkamp, S. Kaganove, and K.R. Mann, *Chem. Mater.*, 2002, **14**(3), 1058.
- M.J. Cich, I.M. Hill, A.D. Lackner, R.J. Martinez, T.C. Ruthenburg, Y. Takeshita, A.J. Young, S.M. Drew, C.E. Buss, and K.R. Mann, *Sens. Act., B: Chem.*, 2010, **149**(1), 199.
- C.E. Buss, and K.R. Mann, *J. Am. Chem. Soc.*, 2002, **124**, 1031.
- S.M. Drew, L.I. Smith, K.A. McGee, and K.R. Mann, *Chem. Mater.*, 2009, **21**, 3117.
- P.J. Martellaro, S.K. Hurst, R. Larson, E.H. Abbott, and E.S. Peterson, *Inorg. Chim. Acta*, 2005, **358**, 3377.
- W.R. Mason and H.B. Gray, *J. Am. Chem. Soc.* 1968, **90**, 5721.
- H. Isci, and W.R. Mason, *Inorg. Chem.* 1974, **13**, 1175.
- H.J. Keller, and R. Lorentz, *J. Organomet. Chem.* 1975, **102**, 119.
- G. Annibale, M. Brandolision, and B. Pitteri, *Polyhedron*, 1995, **14**, 451.
- Siemens SMART Platform CCD, Siemens Industrial Automation, Inc., Madison, WI.
- R. Blessing, *Acta Cryst.* 1995, **A51**, 33.
- G.M. Sheldrick, G. M. 1996, TWINABS V1.02, University of Göttingen, Germany.
- SHELXTL-Plus V5.10, Bruker Analytical X-ray Systems, Madison, WI.
- L.J. Farrugia, 2012, *J. Appl. Cryst.*, **45**, 849.
- Persistence of Vision Raytracer. 2004, Persistence of Vision Pty. Ltd., Williamstown, Victoria, Australia.
- SAINT V6.35A, Bruker Analytical X-Ray Systems, Madison, WI (2002).
- GEMINI, Bruker Analytical X-Ray Systems, Madison, WI (2000).
- STRIP-REDUNDANT V1.1, A program to remove duplicated reflections from HKLF 5 files, W. W. Brennessel and V. G. Young, Jr. (2002).
- SYSABSFILTER V1.1, A program to remove systematic absence violations from HKLF 5 files, W. W. Brennessel and V. G. Young, Jr., (2002).
- Cerius2 V3.0 software; Molecular Simulations Inc., San Diego, CA.
- Beebe, K. R.; Pell, R. J.; Seasholtz, M. B. *Chemometrics: A Practical Guide*, Wiley, New York, 1998, p. 81
- (a) PLATON, A Multipurpose Crystallographic Tool, Utrecht University, Utrecht, The Netherlands, Spek, A. L. 1998 (b) SQUEEZE Sluis, P. v.d.; Spek, A. L. *Acta Cryst.* 1990, **A46**, 194-201.
- Prout, E.G.; Tomkins, F.C.; *Trans. Faraday Soc.* 1944, **40**, 488-498.
- Starbuck, C.; Spartalis, A.; Wai, L.; Wang, J.; Fernandez, P.; Lindemann, C.M.; Zhou, G.X.; Ge, Z. *Cryst. Growth Des.* 2002, **2**, 515; Skrdla, P.J.; Antonucvi, V.; Crocker, L.S.; Wenslow, R.M.; Wright, L.; Zhou, G. J. *Pharm. Biomed. Anal.* 2001, **25**, 731-739.
- Matsuda, Y.; Tatsumi, E.; Chiba, E.; Miwa, Y.; *J. Pharm. Pharmac.* 1975, **28**, 758.
- J.A. Bailey, M.G. Hill, R.E. Marsh, V.M. Miskowski, W.P. Schaefer, and H.B. Gray, *Inorg. Chem.* 1995, **34**, 4591
- R. Zhang, Z. Liang, A. Han, H. Wu, P. Du, W. Lai, and R. Cao, *CrystEngComm*. 2014, **16**, 5531-5542
- R. Hayoun, D.K. Zhong, A.L. Rheingold, and L.H. Doerrer, *Inorg. Chem.* 2006, **45**, 6120
- V. Phillips, K.J. Willard, J.A. Golen, C.J. Moore, A.L. Rheingold, and L.H. Doerrer, *Inorg. Chem.*, 2010, **49**, 9265
- P.W. Du, *Inorg. Chim. Acta*, 2010, **363**, 1355.
- L.J. Grove, J.M. Rennekamp, H. Jude, and W.B. Connick, *J. Am. Chem. Soc.* 2004, **126**, 9; L.J. Grove, A.G. Oliver, J.A. Krause, and W.B. Connick, *Inorg. Chem.* 2008, **47**, 1408.

Graphical Abstract

Mixed cyanide/isocyanide Pt(II) complexes exhibit vapoluminescence. Mechanistic studies of polymorphs and solvates of these complexes indicate large reversible photoluminescence changes accompany inclusion of stoichiometric amounts of water.

